JOURNAL OF COMPUTATIONAL PHYSICS 18, 440–464 (1975)

Flow of Interpenetrating Material Phases*

FRANCIS H. HARLOW AND ANTHONY A. AMSDEN

University of California, Los Alamos Scientific Laboratory, Theoretical Division, Group T-3, Los Alamos, New Mexico 87545

Received February 26, 1975

A previously described numerical technique for the solution of multiphase flow dynamics problems is here both simplified and extended. The simplification cuts down slightly on the momentum coupling among fields, allowing for considerable reduction in complexity of the formulation. The extensions include the capability for compressibility in each material phase, the addition of more interpenetrating fields, and the allowance for motion of a liquid or vapor through a close-packed field of particles. The technique is illustrated by computer-generated plots from a time-varying three-field calculation in a cylindrically symmetric configuration.

INTRODUCTION

The numerical calculation of multiphase fluid flow has been discussed previously [1] for the special case of two phases, one being microscopically incompressible. The calculation technique in that form has proved useful for a variety of studies in which the interpenetrating materials could undergo strong, time-varying distortions in an axisymmetric flow configuration.

For some purposes, for example the safety analysis of a liquid metal cooled fast breeder reactor (LMFBR), the restriction of the numerical technique to handle only two fields of material is not adequate. For other applications it is too restrictive that one of the materials must be completely incompressible. In the process of extending the computer technique to remove these restrictions and add other new capabilities, it soon became apparent that an alternative approach exists for the numerical solution of multiphase fluid flow problems, in which the whole procedure could be appreciably simplified.

It was also apparent that the advantages of this alternative approach might be partially offset by convergence difficulties resulting from a slightly less implicit momentum coupling between fields, which is necessary to achieve the desired

* This work was performed under the auspices of the United States Nuclear Regulatory Commission and the Energy Research and Development Administration.

simplification. We nevertheless constructed a computer code by which to test the new version and have found that the desired advantages can be achieved, and that the anticipated difficulties with convergence can be overcome quite easily.

Accordingly, it is the purpose of this paper to describe the new procedure for multiphase fluid flow calculations, to show the ease by which this version can be applied to circumstances with many simultaneously interpenetrating material phases, to demonstrate its capability for considerably greater flexibility in handling both compressible and incompressible materials, and to show the relative simplicity of the technique.

The Differential Equations

We employ the same nomenclature as in the previous paper [1], in terms of which the differential equations of motion for each of the various fields, or phases, can be written

$$\frac{\partial \rho'}{\partial t} + \nabla \cdot (\rho' \mathbf{u}) = S_\rho , \tag{1}$$

$$\frac{\partial \rho' \mathbf{u}}{\partial t} + \nabla \cdot (\rho' \mathbf{u}\mathbf{u}) = \mathbf{S}_m - \theta \nabla p + \mathbf{V} + \rho' \mathbf{g} + K(\bar{\mathbf{u}} - \mathbf{u}), \tag{2}$$

in which S_ρ and S_m are sources (or sinks) to the mass and momentum of the field resulting from phase transitions, body forces, or other similar effects. Where necessary, we may refer to the field variables of a particular phase by means of subscripts l and n, reserving i and j for use in the finite-difference approximations. For example, θ_l denotes the volume fraction of the lth phase, with

$$\sum_l \theta_l \equiv 1. \tag{3}$$

The mean resistive velocity $\bar{\mathbf{u}}_l$ for a phase, and the effective drag function for that phase, K_l, are defined in terms of binary interactions between phases, K_{ln}, as follows.

$$K_l \equiv \sum_n K_{ln} , \tag{4}$$

$$K_l \bar{\mathbf{u}}_l \equiv \sum_n K_{ln} \mathbf{u}_n . \tag{5}$$

It is essential for momentum conservation that $K_{ln} \equiv K_{nl}$, and the magnitudes of these functions are expected to be positive under all physically realistic circum-

stances. Reference [1] gave an example for the case of particles in a vapor. More generally, we expect

$$K_{ln} = \frac{3}{2}\theta_l\theta_n\left(\frac{1}{r_l}+\frac{1}{r_n}\right)^2\left[\frac{3\mu_l\mu_n}{\mu_l+\mu_n}+\frac{C_{Dln}\rho_l\rho_n \mid \mathbf{u}_l-\mathbf{u}_n \mid r_l r_n}{4(r_l\rho_n+r_n\rho_l)}\right], \tag{6}$$

which reduces to the previous expression in the proper limit, but is also capable of approximating the binary momentum exchange between two fields at various intermediate proportions of mixture. The coefficients C_{Dln} are ordinarily near unity in magnitude.

The microscopic properties of each field are described by an equation of state

$$p_l = f_l(\rho_l, I_l), \tag{7}$$

in which

$$\rho_l \equiv \rho_l'/\theta_l. \tag{8}$$

We have imposed the physically reasonable constraint that $p_l = p$ for all fields; that is, there is local pressure equilibrium among the fields at every instant of time. In the calculation, there is one step, called equilibration, in which this constraint and Eq. (3) are combined to determine the volume fractions for the fields as well as the local, instantaneous pressure. If, for example, the equation of state can be approximated by

$$p = a^2(\rho - \rho_0) + (\gamma - 1)\rho I, \tag{9}$$

then equilibration when a^2 is very large results in a microscopic density that remains very close to ρ_0, and the dynamics of that phase behaves as though the material were essentially incompressible. For practical calculations, it is important to allow for much more general equations of state than the form in Eq. (9), and we have found it advantageous to write our present computer code with a separate equation-of-state section to allow for maximum flexibility in this regard, which also calculates $\partial p/\partial\rho$, exemplified in the following equations by $a^2 + (\gamma - 1)I$.

We have, in addition, an equation for each field or phase describing the transport of specific internal energy, I, which we have found appropriate to write in the following form.

$$\frac{\partial(\rho' I)}{\partial t} + \nabla\cdot(\mathbf{u}\rho' I) = \frac{\theta p}{\rho}\left[\frac{\partial\rho}{\partial t} + \mathbf{u}\cdot\nabla\rho\right] + S_i + R(\bar{T} - T) + \Lambda + V_i + \nabla\cdot(k\theta\nabla T). \tag{10}$$

S_i is a source function describing the generation of internal energy from phase

transitions, chemical sources or sinks, and similar processes. R is an exchange function to the mean exchange temperature for that field. Again, we assume binary processes, for which

$$R_l \equiv \sum_n R_{nl}\,, \tag{11}$$

$$R_l \bar{T}_l \equiv \sum_n R_{nl} T_n\,. \tag{12}$$

The heat conduction term utilizes a coefficient, k, which must vanish whenever the phase becomes disperse, that is, the volume fraction becomes small. The dissipative term, Λ, represents the rate of internal energy production as a result of momentum exchange. The total rate from this process for all the fields is

$$\bar{\Lambda} = \tfrac{1}{2} \sum_n \sum_l K_{nl}(\mathbf{u}_l - \mathbf{u}_n) \cdot (\mathbf{u}_l - \mathbf{u}_n), \tag{13}$$

which we partition among fields

$$\Lambda_l = \lambda_l \bar{\Lambda}, \tag{14}$$

with weighting coefficients, λ_l, that depend on local conditions and must satisfy the constraint

$$\sum_l \lambda_l \equiv 1. \tag{15}$$

Numerical Procedure

As in Ref. [1], we introduce an Eulerian mesh of computational cells for the representation of data describing the field variables, and for the approximation of the differential equations by finite difference representations. Field variables centered in the rectangular cells include the density, pressure, and internal energy of each phase. The cell-centered variables are labeled with indices i and j, counting cell numbers in the r and z directions, respectively. The fluid velocities, in contrast, are centered on the sides of the cell and labeled with half-integer indices. For example, $u^j_{i+(1/2)}$ is the radial velocity, located on the right face of the cell, and $v_i^{j+(1/2)}$ is the axial velocity, located on the top face of the cell.

For any cell-centered quantity, $Q_i{}^j$, the convective flux through the side of the cell is given by the product of the normal component of velocity and the quantity, for example $(uQ)^j_{i+(1/2)}$. In a form that combines both centered and donor-cell properties, we change this flux expression to

$$\langle uQ \rangle^j_{i+(1/2)} \equiv u^j_{i+(1/2)}[(\tfrac{1}{2} + \xi)\, Q_i{}^j + (\tfrac{1}{2} - \xi)\, Q^j_{i+1}], \tag{16}$$

in which the value of ξ is controlled by the specified parameters, α_0 and β_0, which have magnitudes lying between zero and 0.5, and

$$\xi \equiv (\beta_0 u^j_{i+(1/2)}\, \delta t)/\delta r + \alpha_0 \operatorname{sign}(u^j_{i+(1/2)}). \tag{17}$$

For each of the fields in a computational cell we approximate the components of the viscous stress terms in Eq. (2) by

$$(V_r)^j_{i+(1/2)} = \frac{\nu_s}{\delta r^2}\left\{\frac{(\rho')^j_{i+1}}{r_{i+1}}[(ru)^j_{i+(3/2)} - (ru)^j_{i+(1/2)}] - \frac{(\rho')_i{}^j}{r_i}[(ru)^j_{i+(1/2)} - (ru)^j_{i-(1/2)}]\right\}$$
$$+ \frac{\nu_s}{\delta z^2}\{(\rho')^{j+(1/2)}_{i+(1/2)}[u^{j+1}_{i+(1/2)} - u^j_{i+(1/2)}] - (\rho')^{j-(1/2)}_{i+(1/2)}[u^j_{i+(1/2)} - u^{j-1}_{i+(1/2)}]\}, \tag{18}$$

and

$$(V_z)^{j+(1/2)}_i = \frac{\nu_s}{r_i\,\delta r^2}\{(\rho')^{j+(1/2)}_{i+(1/2)}\, r_{i+(1/2)}[v^{j+(1/2)}_{i+1} - v^{j+(1/2)}_i]$$
$$- (\rho')^{j+(1/2)}_{i-(1/2)}\, r_{i-(1/2)}[v^{j+(1/2)}_i - v^{j+(1/2)}_{i-1}]\}$$
$$+ \frac{\nu_s}{\delta z^2}\{(\rho')^{j+1}_i[v^{j+(3/2)}_i - v^{j+(1/2)}_i] - (\rho')_i{}^j[v^{j+(1/2)}_i - v^{j-(1/2)}_i]\}. \tag{19}$$

In this form, the purpose of viscosity is to damp the high-frequency oscillations that cannot be resolved or would lead to numerical instability, but the magnitude of ν_s, the specified kinematic viscosity coefficient, must not be so great as to appreciably damp the larger-scale flow instabilities of physical interest [2].

We define, for each field, the quantities

$$\overline{(\rho' u)}^j_{i+(1/2)} = (\rho' u)^j_{i+(1/2)} + (V_r)^j_{i+(1/2)}\, \delta t + \frac{\delta t}{r_{i+(1/2)}\,\delta r}[\langle \rho' u^2 r\rangle_i{}^j - \langle \rho' u^2 r\rangle^j_{i+1}]$$
$$+ (S_{mr})^j_{i+(1/2)}\, \delta t + \frac{\delta t}{\delta z}[\langle \rho' uv\rangle^{j-(1/2)}_{i+(1/2)} - \langle \rho' uv\rangle^{j+(1/2)}_{i+(1/2)}], \tag{20}$$

and

$$\overline{(\rho' v)}^{j+(1/2)}_i = (\rho' v)^{j+(1/2)}_i + (V_z)^{j+(1/2)}_i\, \delta t + \frac{\delta t}{r_i\,\delta r}[\langle \rho' uvr\rangle^{j+(1/2)}_{i-(1/2)} - \langle \rho' uvr\rangle^{j+(1/2)}_{i+(1/2)}]$$
$$+ (S_{mz})^{j+(1/2)}_i\, \delta t + \frac{\delta t}{\delta z}[\langle \rho' v^2\rangle_i{}^j - \langle \rho' v^2\rangle^{j+1}_i]. \tag{21}$$

With these shorthand expressions, the finite-difference approximations to Eq. (2) become

$${}^{n+1}(\rho' u)^j_{i+(1/2)} = \overline{(\rho' u)}^j_{i+(1/2)} + K^j_{i+(1/2)}\, \delta t({}^{n+1}\bar{u}^j_{i+(1/2)} - {}^{n+1}u^j_{i+(1/2)})$$
$$- \theta^j_{i+(1/2)}\, \delta t({}^{n+1}p^j_{i+1} - {}^{n+1}p_i{}^j)/\delta r, \tag{22}$$

and

$$ {}^{n+1}(\rho' v)_i^{j+(1/2)} = \overline{(\rho' v)}_i^{j+(1/2)} + K_i^{j+(1/2)}\,\delta t({}^{n+1}\bar{v}_i^{j+(1/2)} - {}^{n+1}v_i^{j+(1/2)}) $$
$$ - \theta_i^{j+(1/2)}\,\delta t({}^{n+1}p_i^{j+1} - {}^{n+1}p_i^{j})/\delta z. \tag{23} $$

In similar fashion, Eq. (1) becomes

$$ {}^{n+1}D_i^j \equiv [{}^{n+1}(\rho')_i^j - {}^{n}(\rho')_i^j]/\delta t + [{}^{n+1}\langle \rho' ur\rangle_{i+(1/2)}^j - {}^{n+1}\langle \rho' ur\rangle_{i-(1/2)}^j]/(r_i\,\delta r) $$
$$ + [{}^{n+1}\langle \rho' v\rangle_i^{j+(1/2)} - {}^{n+1}\langle \rho' v\rangle_i^{j-(1/2)}]/\delta z - (S_\rho)_i^j = 0. \tag{24} $$

The left superscript, n or $n+1$, counts time cycles; where omitted, time cycle n is implied.

With the equations written in this fashion, we can outline the solution procedure in terms of the following steps.

1. As a result of calculations from the previous cycle or the specification of initial conditions, the computer memory contains for every computational cell the field variables for each material phase in that cell. Since the mass and momentum equations have been written in an implicit formulation, their solutions will be obtained by iteration. (The internal energy calculations are postponed to the last part of each cycle, where they are performed explicitly.) Each complete iteration consists of two basic parts, the first treating the material phases in each cell independently, and the second performing a pressure equilibration among phases. In this first step, the various field variable values are initialized.

2. For each of the material phases, a value of D is calculated from Eq. (24), which in turn enters a Newton–Raphson formula for the determination of an increment to the pressure variable. By means of the equation of state, the revised density of the cell is calculated for each phase.

3. Adjustments to the volume fraction for each phase are calculated in order to bring the pressures into local equilibrium. If the material of a phase is granular or particulate, and capable of close packing, then its pressure is not equilibrated to that of the other materials for those computational cells in which the volume fraction of the material equals (or exceeds) the specified magnitude for close packing. The pressure in the close-packed field allows its contortions to proceed with little or no further compression depending on the equation of state of the close-packed phase, while the independent pressure field for the interpenetrating phases allows for their continuing permeation.

4. The equilibrated pressures are used to calculate the material velocities for each phase.

In these steps, the essential difference from the previous technique [1] is apparent. There, because of completely implicit momentum coupling among fields, the material phases in each cell could not be treated independently, leading to equations of considerable complexity, which would be difficult to extend to the case of many different material phases per cell.

Steps 2–4 of the iteration are repeated until the value of D is sufficiently small, at which stage the iteration is considered to have converged. Throughout this process, the $n + 1$ values in the finite-difference equations are replaced by those same quantities symbolized by a tilde over each.

To initialize the field variables that will be adjusted during the iterations (step 1, above) we first calculate the pressure for each material phase that is not close packed by means of the equation of state, using the updated internal energy, which was calculated *after* the pressure equilibration in the previous cycle, so that at this stage, there is no longer a precise local pressure equilibrium. Then the velocity components are initialized by

$$\tilde{u}^j_{i+(1/2)} = \frac{\overline{(\rho' u)}^j_{i+(1/2)} + ({}^n\theta^j_{i+(1/2)}\,\delta t/\delta r)(\tilde{p}_i{}^j - \tilde{p}^j_{i+1}) + (K\bar{u})^j_{i+(1/2)}\,\delta t}{{}^n(\rho')^j_{i+(1/2)} + K^j_{i+(1/2)}\,\delta t}, \tag{25}$$

and

$$\tilde{v}^{j+(1/2)}_i = \frac{\overline{(\rho' v)}^{j+(1/2)}_i + ({}^n\theta^{j+(1/2)}_i\,\delta t/\delta z)(\tilde{p}_i{}^j - \tilde{p}^{j+1}_i) + (K\bar{v})^{j+(1/2)}_i\,\delta t}{{}^n(\rho')^{j+(1/2)}_i + K^{j+(1/2)}_i\,\delta t}. \tag{26}$$

Next, the density and void fraction values are initialized by

$$(\tilde{\rho}')_i{}^j = ({}^n\rho')_i{}^j - \delta t \left\{ \frac{1}{r_i\,\delta r} [\langle \tilde{\rho}' \tilde{u} r \rangle^j_{i+(1/2)} - \langle \tilde{\rho}' \tilde{u} r \rangle^j_{i-(1/2)}] + \frac{1}{\delta z} [\langle \tilde{\rho}' \tilde{v} \rangle^{j+(1/2)}_i - \langle \tilde{\rho}' \tilde{v} \rangle^{j-(1/2)}_i] \right\}, \tag{27}$$

and

$$\tilde{\theta}_i{}^j = (\tilde{\rho}')^j_i/\rho_0\,, \tag{28}$$

the latter being calculated only for those fields that are close packed, that is, for which the new value of θ from Eq. (28) exceeds the specified volume fraction at which the particles or granules of the field are touching each other. The fields that are not close packed are then equilibrated in pressure to determine their volume fractions, which must add up to the total volume fraction allowed by the close-packed fields. This completes the initialization for iteration.

The iterative steps commence with a calculation of $\tilde{D}$ for each material phase. If the material is not close packed,

$$\tilde{D}_i^j = \frac{1}{\delta t}[(\tilde{\rho}')_i^j - {}^n(\rho')_i^j] + \frac{1}{r_i\,\delta r}[\langle\tilde{\rho}'\tilde{u}r\rangle_{i+(1/2)}^j - \langle\tilde{\rho}'\tilde{u}r\rangle_{i-(1/2)}^j] + \frac{1}{\delta z}[\langle\tilde{\rho}'\tilde{v}\rangle_i^{j+(1/2)} - \langle\tilde{\rho}'\tilde{v}\rangle_i^{j-(1/2)}] - S_\rho\,. \tag{29}$$

If it is close packed, and essentially incompressible,

$$\tilde{D}_i^j = (\tilde{\rho}')_i^j\left\{\frac{1}{r_i\,\delta r}[\tilde{u}_{i+(1/2)}^j r_{i+(1/2)} - \tilde{u}_{i-(1/2)}^j r_{i-(1/2)}] + \frac{1}{\delta z}[\tilde{v}_i^{j+(1/2)} - \tilde{v}_i^{j-(1/2)}]\right\}. \tag{30}$$

For close-packed fields in which the compressibility is important (e.g., for the propagation of shocks or rarefactions through the touching granules), Eq. (29) is used, but in such a case the time step per cycle will usually have to be very much smaller in order to resolve the dynamics.

With a specified value for the over/under relaxation parameter, ω, the pressure increment for each field is

$$\delta\tilde{p}_i^j = -\omega\beta_i^j\tilde{D}_i^j, \tag{31}$$

in which

$$\frac{1}{\beta_i^j} = \frac{1}{[a^2 + (\gamma-1)\,I_i^j]\,\delta t} + \frac{\delta t}{r_i\,\delta r}\left[\frac{r_{i+(1/2)}\theta_{i+(1/2)}^j + r_{i-(1/2)}\theta_{i-(1/2)}^j}{\delta r} - r_{i+(1/2)}K_{i+(1/2)}^j\left(\frac{\partial\tilde{u}_{i+(1/2)}^j}{\partial\tilde{p}_i{}^j}\right) + r_{i-(1/2)}K_{i-(1/2)}^j\left(\frac{\partial\tilde{u}_{i-(1/2)}^j}{\partial\tilde{p}_i{}^j}\right)\right] + \frac{\delta t}{\delta z}\left[\frac{\theta_i^{j+(1/2)} + \theta_i^{j-(1/2)}}{\delta z} - K_i^{j+(1/2)}\left(\frac{\partial\tilde{v}_i^{j+(1/2)}}{\partial\tilde{p}_i{}^j}\right) + K_i^{j-(1/2)}\left(\frac{\partial\tilde{v}_i^{j-(1/2)}}{\partial\tilde{p}_i{}^j}\right)\right], \tag{32}$$

with

$$\frac{\partial\tilde{u}_{i+(1/2)}^j}{\partial\tilde{p}_i{}^j} = \frac{\theta_{i+(1/2)}^j(\delta t/\delta r) - \{\tilde{u}_{i+(1/2)}^j/[a^2 + (\gamma-1)\,I_{i+(1/2)}^j]\}}{(\rho')_{i+(1/2)}^j + K_{i+(1/2)}^j\,\delta t},$$

$$\frac{\partial\tilde{u}_{i-(1/2)}^j}{\partial\tilde{p}_i{}^j} = \frac{-\theta_{i-(1/2)}^j(\delta t/\delta r) - \{\tilde{u}_{i-(1/2)}^j/[a^2 + (\gamma-1)\,I_{i-(1/2)}^j]\}}{(\rho')_{i-(1/2)}^j + K_{i-(1/2)}^j\,\delta t},$$

$$\frac{\partial \tilde{v}_i^{j+(1/2)}}{\partial \tilde{p}_i{}^j} = \frac{\theta_i^{j+(1/2)}(\delta t/\delta z) - \{\tilde{v}_i^{j+(1/2)}/[a^2 + (\gamma - 1)\, I_i^{j+(1/2)}]\}}{(\rho')_i^{j+(1/2)} + K_i^{j+(1/2)}\, \delta t}.$$

and

$$\frac{\partial \tilde{v}_i^{j-(1/2)}}{\partial \tilde{p}_i{}^j} = \frac{-\theta_i^{j-(1/2)}(\delta t/\delta z) - \{\tilde{v}_i^{j-(1/2)}/[a^2 + (\gamma - 1)\, I_i^{j-(1/2)}]\}}{(\rho')_i^{j-(1/2)} + K_i^{j-(1/2)}\, \delta t}.$$

From this updated pressure for each field, the density, ρ', is calculated, using the equation of state and the value of θ from the previous equilibration or the initialization. With ρ' held fixed for each field, the pressure is equilibrated among the fields that are not close packed. This results in a consistent set of new values for the volume fractions, which in turn can then be used to update the velocity components for each field,

$$(\tilde{u})_{i+(1/2)}^j = \frac{\overline{(\rho' u)}_{i+(1/2)}^j + (\tilde{\theta}_{i+(1/2)}^j\, \delta t/\delta r)(\tilde{p}_i{}^j - \tilde{p}_{i+1}^j) + (K\tilde{\tilde{u}})_{i+(1/2)}^j\, \delta t}{(\tilde{\rho}')_{i+(1/2)}^j + K_{i+(1/2)}^j\, \delta t}, \tag{33}$$

$$(\tilde{v})_i^{j+(1/2)} = \frac{(\rho' v)_i^{j+(1/2)} + (\tilde{\theta}_i^{j+(1/2)}\, \delta t/\delta z)(\tilde{p}_i{}^j - \tilde{p}_i^{j+1}) + (K\tilde{\tilde{v}})_i^{j+(1/2)}\, \delta t + (\rho')_i^{j+(1/2)} g\, \delta t}{(\tilde{\rho}')_i^{j+(1/2)} + K_i^{j+(1/2)}\, \delta t}. \tag{34}$$

Finally, as a last step in the iteration, and in preparation for the next iteration, we calculate

$$(K\tilde{\tilde{u}}_1)_{i+(1/2)}^j = [K_{12}\tilde{u}_2 + K_{13}\tilde{u}_3]_{i+(1/2)}^j, \qquad (K\tilde{\tilde{v}}_1)_i^{j+(1/2)} = [K_{12}\tilde{v}_2 + K_{13}\tilde{v}_3]_i^{j+(1/2)},$$

$$(K\tilde{\tilde{u}}_2)_{i+(1/2)}^j = [K_{12}\tilde{u}_1 + K_{23}\tilde{u}_3]_{i+(1/2)}^j, \qquad (K\tilde{\tilde{v}}_2)_i^{j+(1/2)} = [K_{12}\tilde{v}_1 + K_{23}\tilde{v}_3]_i^{j+(1/2)},$$

$$(K\tilde{\tilde{u}}_3)_{i+(1/2)}^j = [K_{13}\tilde{u}_1 + K_{23}\tilde{u}_2]_{i+(1/2)}^j, \qquad (K\tilde{\tilde{v}}_3)_i^{j+(1/2)} = [K_{13}\tilde{v}_1 + K_{23}\tilde{v}_2]_i^{j+(1/2)}.$$

If these quantities were to be calculated *simultaneously* with Eqs. (33) and (34), the necessary formulation, like that of the previous technique [1], would be considerably more complicated and much less flexible, especially in regard to the addition of more fields to the calculation.

When the iteration has converged, according to some appropriate measure of the smallness of $\tilde{D}$ for all cells, then the internal energy of each material phase is calculated explicitly. This requires the density for each field from the previous

cycle, in order to evaluate $\partial\rho/\partial t$. The form we use at present for the internal energy equation is

$$
\begin{aligned}
{}^{n+1}(\rho' I)_i^j = {}^n(\rho' I)_i^j &+ \frac{\delta t}{r_i\,\delta r}\left[\langle \rho' Iur\rangle_{i-(1/2)}^j - \langle \rho' Iur\rangle_{i+(1/2)}^j\right] \\
&+ \frac{\delta t}{\delta z}\left[\langle \rho' Iv\rangle_i^{j-(1/2)} - \langle \rho' Iv\rangle_i^{j+(1/2)}\right] \\
&+ \frac{\theta_i^j p_i^j\,\delta t}{\rho_i^j}\left\{\frac{{}^{n+1}\rho_i^j - {}^n\rho_i^j}{\delta t} + \frac{1}{r_i\,\delta r}\left[\langle \rho ur\rangle_{i+(1/2)}^j - \langle \rho ur\rangle_{i-(1/2)}^j\right]\right. \\
&+ \frac{1}{\delta z}\left[\langle \rho v\rangle_i^{j+(1/2)} - \langle \rho v\rangle_i^{j-(1/2)}\right] \\
&\left. - \rho_i^j\left[\frac{(ru)_{i+(1/2)}^j - (ru)_{i-(1/2)}^j}{r_i\,\delta r} + \frac{v_i^{j+(1/2)} - v_i^{j-(1/2)}}{\delta z}\right]\right\} \\
&+ \delta t\left\{\left[(S_i)_i^j + \Lambda_i^j + (V_i)_i^j\right]\right. \\
&+ \frac{1}{r_i\,\delta r^2}\left[r_{i+(1/2)}(k\theta)_{i+(1/2)}^j\,(T_{i+1}^j - T_i^j) - r_{i-(1/2)}(k\theta)_{i-(1/2)}^j\,(T_i^j - T_{i-1}^j)\right] \\
&\left. + \frac{1}{\delta z^2}\left[(k\theta)_i^{j+(1/2)}\,(T_i^{j+1} - T_i^j) - (k\theta)_i^{j-(1/2)}\,(T_i^j - T_i^{j-1})\right]\right\} \\
&+ R_i^j\,\delta t(\bar{T}_i^j - T_i^j). \qquad (35)
\end{aligned}
$$

The latest updated values should be used throughout, where available, except for the term ${}^n\rho_i^j$. We have found it necessary to repeat the calculation in Eqs. (27) and (28) after the iteration has converged, but before the convection of internal energy is calculated in Eq. (35). The work term in Eq. (10) has been written in a somewhat different form to facilitate donor-cell differencing.

Equilibration

The technique for bringing the pressures of all fields into local equilibrium is simple if the equation of state for every material phase is linear in the density. More generally, the equilibration can be accomplished by iteration. Let

$$Q_n \equiv p - f_n(\rho_n, I_n).$$

Our problem is to find the zeros of the Q_n functions, solving for a set of θ_n values, subject to Eqs. (3) and (8). For this purpose, let

$$y_n \equiv (\rho_n'/\theta_n^2)(\partial f_n/\partial \rho_n).$$

Through the iterative sequence, θ_n remains unchanged for every close-packed field. For the non-close-packed, or open, fields we start with an initial guess for p and the θ_n values. With sums that include only the open fields, each iteration changes the result from the previous one by amounts

$$\delta p = \left[\sum \theta_n - \theta_0 - \sum (Q_n/y_n)\right] \Big/ \sum (1/y_n)$$

and

$$\delta\theta = -(Q_n + \delta p)/y_n ,$$

in which θ_0 is the volume fraction not occupied by the close-packed fields.

Experience shows that this iterative procedure converges very quickly for any set of well-behaved material phases.

One restriction on this present technique can be illustrated by the effect on equilibration of having all fields nearly incompressible. Because the calculation of ρ' values for each field is independent of the processes occurring in the other fields, except for equilibration, it is possible to enter this section with a small amount more or less of total mass in a cell than would be possible at normal microscopic density, so that equilibration will result in a corresponding departure in each field from that density, with consequent strong departures in pressure from the values expected in the ordinary course of a calculation. Thus we see that relaxation of the degree of implicitness in this present numerical procedure means that in every computational cell there must be an appreciable amount of at least one highly compressible field.

Automatic Time Step and Dissipation Control

Because of the implicit formulation of the equations, the time increment per computational cycle, δt, is not limited by the usual Courant condition, which becomes highly restrictive as the local sound speed becomes large. For accuracy, however, it is necessary to impose a modified Courant condition, based on the maximum fluid speed in the system, u_m . Indeed, we use this condition to determine δt each cycle, in such a way that

$$u_m \, \delta t/\delta x = f, \tag{36}$$

where δx is the smaller of δr and δz and f is a specified number with magnitude somewhat less than unity. Actually, it is sufficient, and sometimes less restrictive, to calculate $u_m/\delta x$ as the maximum among all values of $u/\delta r$ and $v/\delta z$

simple form. Donor-cell flux calculations also help to automatically control

dissipation, but the much more general technique of complete local truncation-error correction [3, 4] is not incorporated into the technique at present.

To estimate the necessary magnitude of ν_s for Eqs. (18) and (19), we use the results of Hirt [3] to show that

$$\nu_s \approx (u_m \, \delta x/2)[\tfrac{1}{2} + (u_m \, \delta t/\delta x)],$$

or, with Eq. (36)

$$\nu_s = f(f + \tfrac{1}{2}) \, \delta x^2/(2\delta t).$$

To avoid diffusional instability, we also require

$$4\nu_s \, \delta t < \delta x^2,$$

which is automatically satisfied, provided $f < \frac{1}{2}$. We have obtained satisfactory results using $f = \frac{1}{4}$, which simultaneously ensures sufficiently small fluid motion per cycle and adequate dissipation, while precluding diffusional instability and excessive damping. Any improvements over this simple procedure would require the very complicated procedures of local truncation error subtraction [4], which, however, would be recommended to anyone seeking the greatest possible resolution of flow details.

Iteration Convergence Rate

A major difference between the present technique and the one we previously described [1] is partial rather than complete implicitness of the momentum exchange between fields. The advantages of the partially implicit treatment include the relative decoupling of the equations in the iterative solution phase, and the resulting simplifications and ease of extension to allow for many fields.

The contrast between the two approaches can be illustrated by a careful consideration of Eq. (22). For our purpose it is sufficient to consider the following simplified version of that equation, which, for the first field of a two-field calculation becomes

$$u_1^{h+1} = A_1 + B_1(\bar{u}_1^{\,h} - u_1^{h+1}),$$

in which $B_1 \equiv K \, \delta t/\rho_1'$ and A_1 contains the remaining terms. The index, h, counts iteration number; as $h \to \infty$, the terms with h or $h + 1$ approach the $n + 1$ values if the iteration converges. For this two-field illustration, $\bar{u}_1 \equiv u_2$, and the pair of equations becomes

$$u_1^{h+1} = A_1 + B_1(u_2^{\,h} - u_1^{h+1}), \tag{37}$$

$$u_2^{h+1} = A_2 + B_2(u_1^{\,h} - u_2^{h+1}). \tag{38}$$

In our previous technique [1], the h-level quantities were replaced by their counterparts at the $h + 1$ level, in which case the two equations could not be solved separately, as above, but required a simultaneous solution, namely,

$$u_n^{\infty} = (A_n + A_1B_2 + A_2B_1)/(1 + B_1 + B_2). \tag{39}$$

In the actual case, with pressures and density also varying during the iterations, this simple simultaneous solution becomes vastly more complicated. Our purpose here, however, is to show the manner in which the iterative solution of Eqs. (37) and (38) approaches the result in Eq. (39), since this result bears directly on the way in which our partially implicit multiphase technique converges.

To perform the analysis, let $u_n^{h+1} \equiv u_n^{\infty} + \epsilon_n^{h+1}$. Then one can show that

$$\epsilon_1^{h+1} = B_1\epsilon_2{}^h/(1 + B_1),$$

and

$$\epsilon_2^{h+1} = B_2\epsilon_1{}^h/(1 + B_2).$$

Suppose that each error decreases by a factor F during the iteration, that is, $\epsilon_n^{h+1} = F\epsilon_n{}^h$. Then

$$F = [B_1B_2/(1 + B_1)(1 + B_2)]^{1/2}, \tag{40}$$

and it is this result that indicates the convergence-rate effect on our new technique from the partial implicitness of the momentum coupling. As long as the value of F, which can be controlled by the magnitude of δt, is sufficiently smaller than unity, then rapid convergence is ensured. In particular, we automate the calculation to include a δt control that overrides the one in the previous section, to force $F \lesssim 0.5$ whenever necessary. Experience shows that this cutoff choice allows for rapid convergence insofar as the momentum coupling effects are concerned. We also have seen that little loss in computer running time would result from a cutoff at $F \lesssim 0.25$, since the effect of decreased time step per cycle is nearly compensated by the smaller number of iterations per cycle required for convergence. In case the δt required for control of F is smaller than that of the previous section by more than a factor of 10, the calculation warns against possible convergence inefficiency and recommends a review of the K formulation. Since $K\,\delta t/\rho'$ measures the ratio of δt to the relaxation time for the velocity difference between fields, its value need not greatly exceed unity for any problem of physical interest. Thus, inefficiency from F control can be eliminated by a ceiling on the K functions. This should not introduce errors in the physical representation, because fields that are already tightly tied to each other cannot behave with appreciable difference as a function of the tying strength.

Example of a Test Calculation

The following example serves to illustrate some of the features of the numerical technique. A wealth of information in both printed and visual form is available for analysis from the computer runs. The geometries of the actual application problems can be quite complicated, but we have chosen a highly simplified example to illustrate the capability for a fully three-field calculation.

In preparation for the study of possible core disassembly accidents in the LMFBR, we have simulated the case of an idealized mockup of the reactor. The calculation follows the dynamics of three fields of material: (1) vapor, (2) fuel, and (3) iron. The vapor field is fully compressible, and is composed of a homogeneous mixture of the vapors of coolant, fuel, and iron. The fuel and iron fields have much higher sound speeds than the vapor, and therefore behave microscopically as though they were nearly incompressible. The schematic in Fig. 1 shows a central core (I), containing primarily vapor and dispersed fuel, an iron liner (II), which is initially close packed, although devoid of strength effects, and permeated with vapor, and an overhead region (III) of essentially pure vapor. The vapor in region I is heated and under pressure; the other two regions are relatively cool and in pressure equilibrium. The computing mesh is a confining system, bounded by an axis of cylindrical symmetry along the left, and rigid freeslip walls along the other three sides.

Microfilm plots of computer results are shown in Figs. 2 through 5, in which each set of four plots is a sequence for a particular quantity, at nondimensional problem times 0.1, 50, 100, and 200 units, reading left to right, then down. The time 0.1, which is at the end of the first calculation cycle, exhibits the initial trends of velocity and pressure.

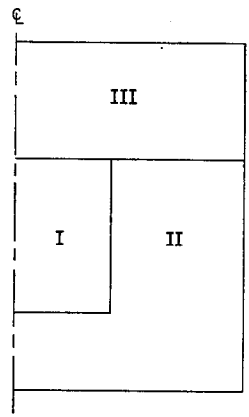

Fig. 1. Schematic of the flow regions of the computing mesh.

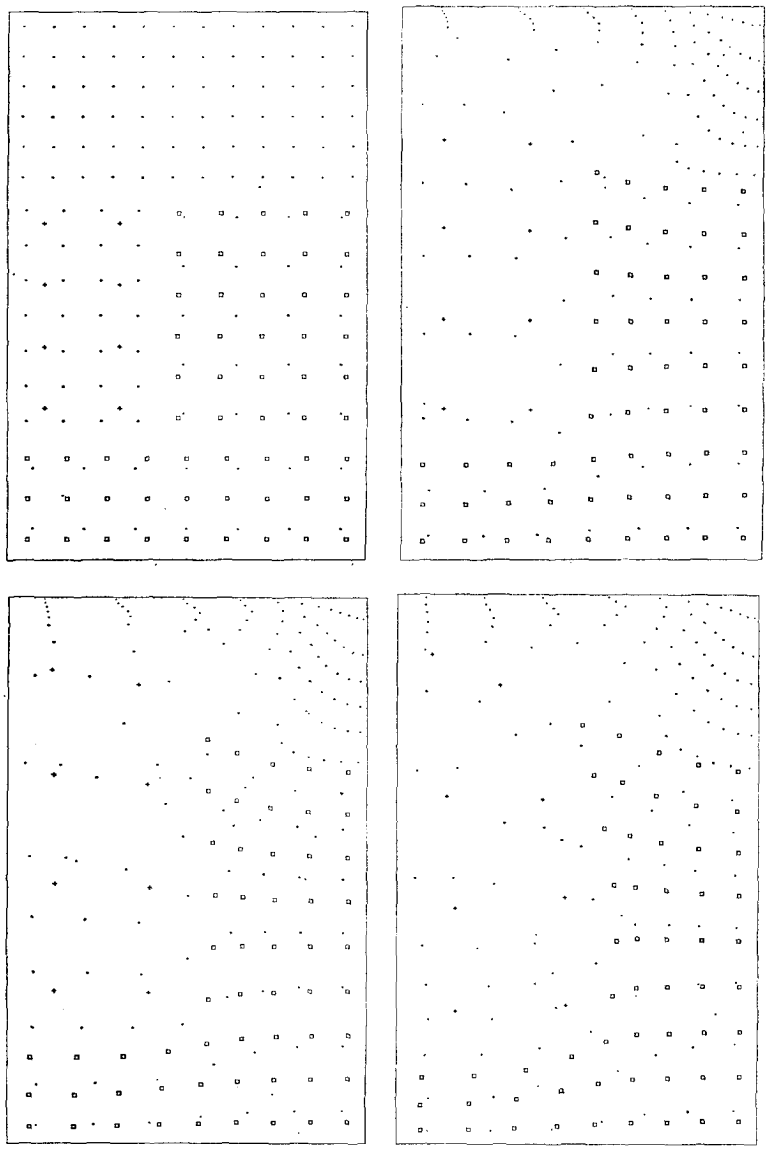

FIG. 2. Marker particle plots, at problem times 0.1, 50, 100, and 200, reading left to right and then down. Field 1 is represented by light dots, field 2 by crosses, and field 3 by open squares.

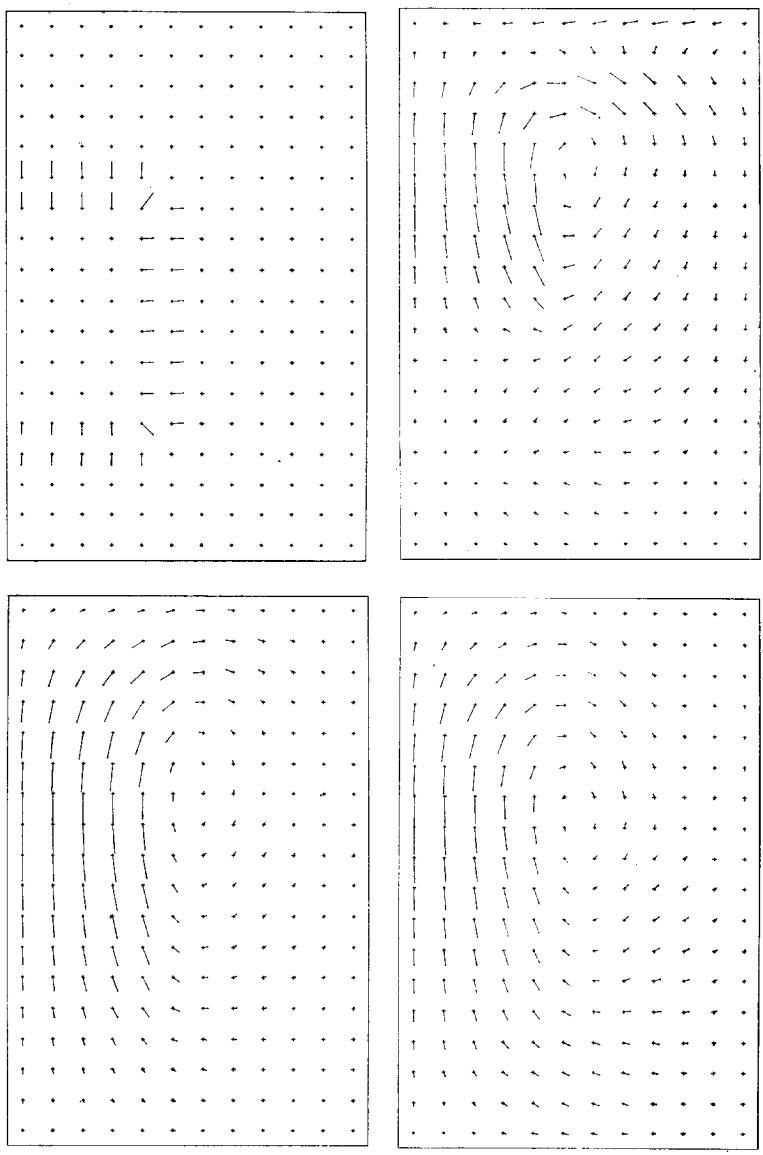

FIG. 3a. Velocity vectors for field 1. Within each sequence, the problem times are the same as those of Fig. 2.

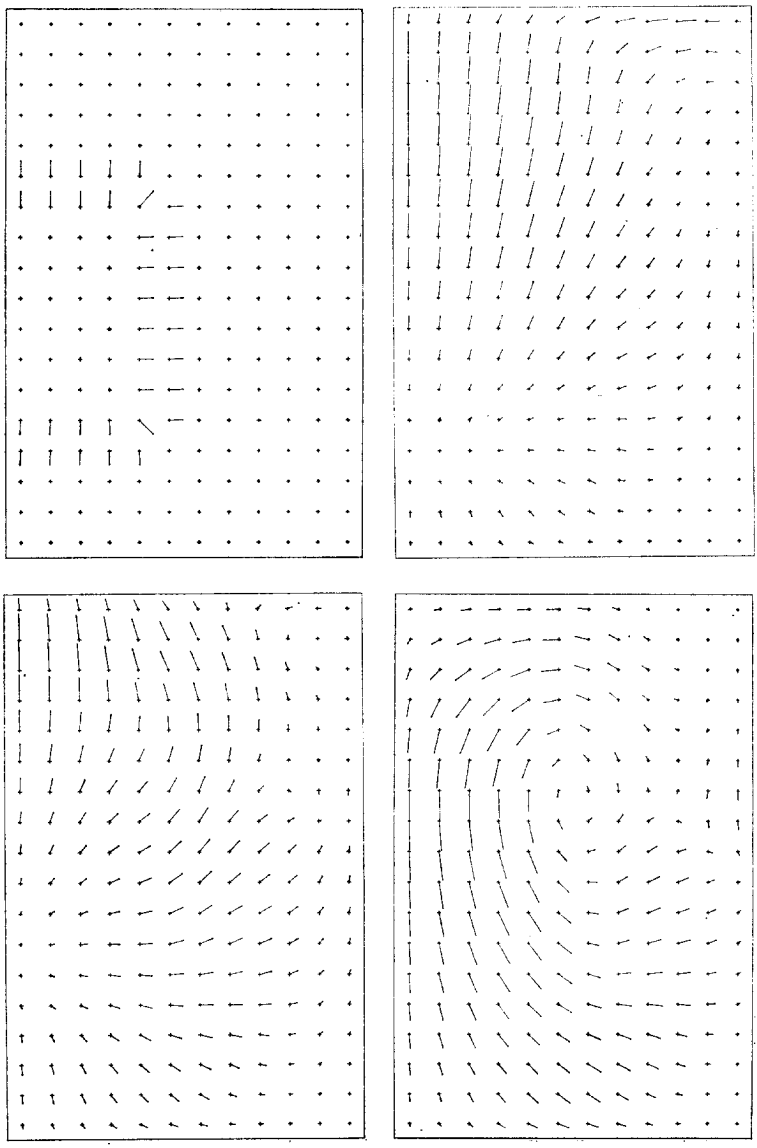

FIG. 3b. Velocity vectors for field 2. Within each sequence, the problem times are the same as those of Fig. 2.

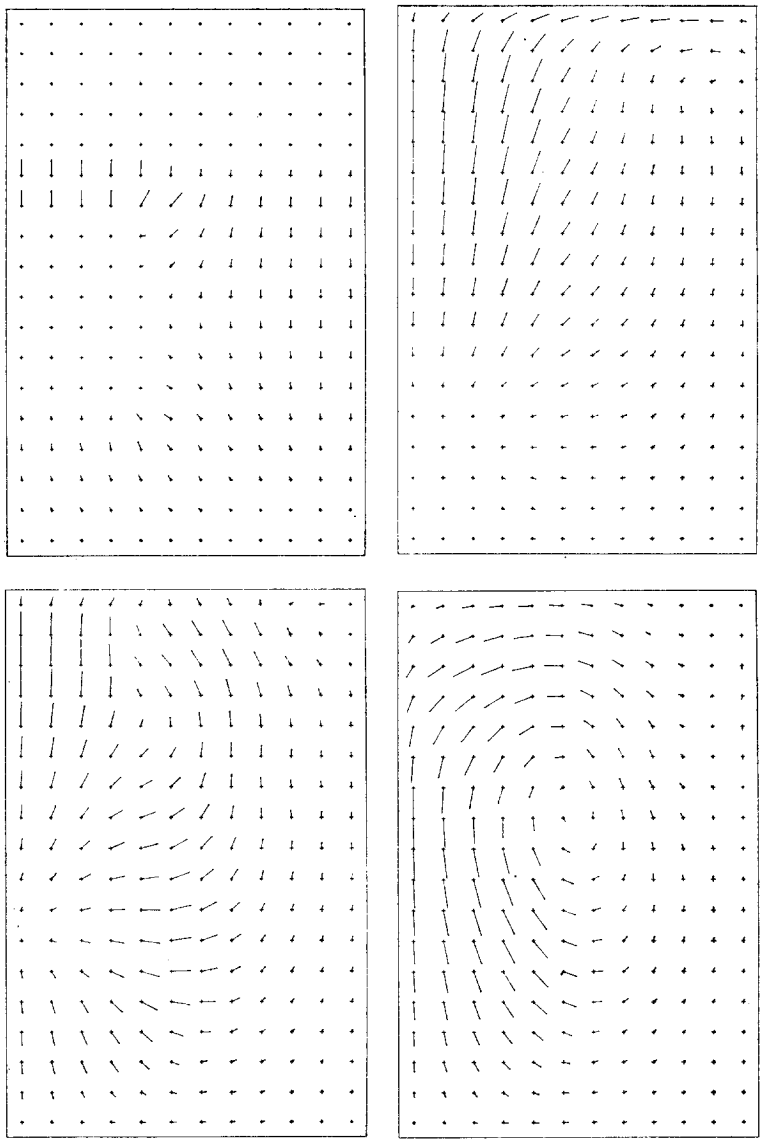

FIG. 3c. Velocity vectors for field 3. Within each sequence, the problem times are the same as those of Fig. 2.

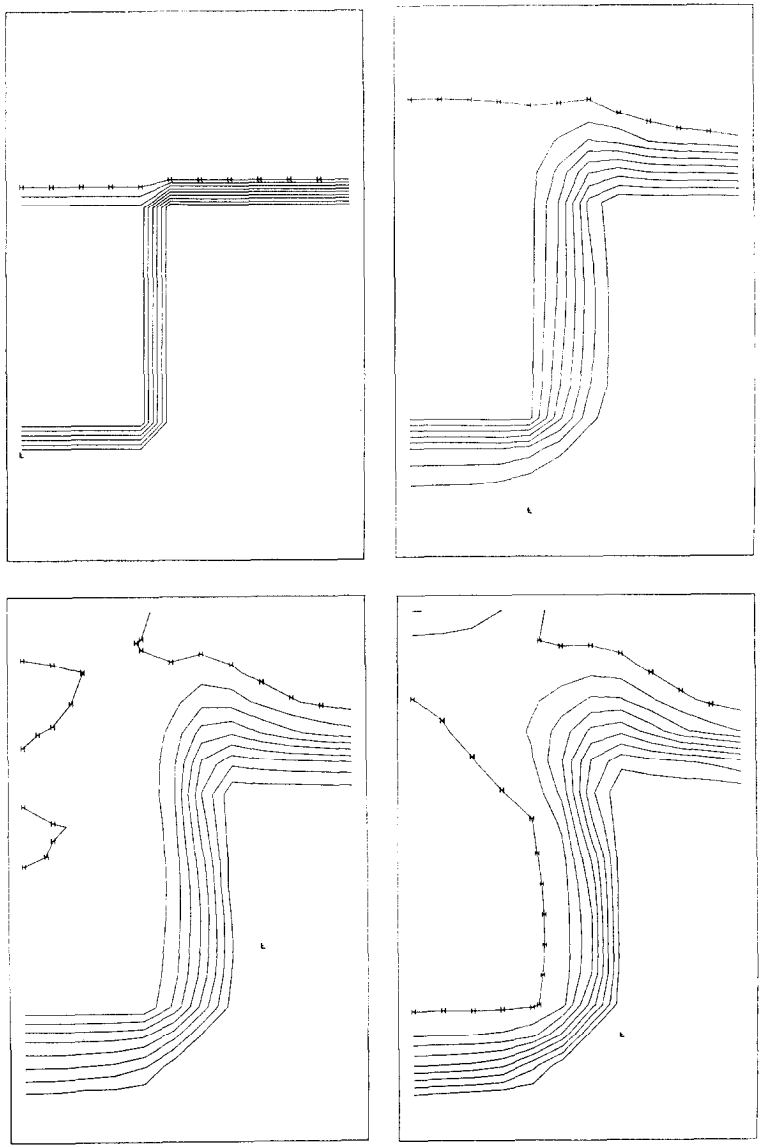

FIG. 4a. Plots of volume fraction θ for field 1.

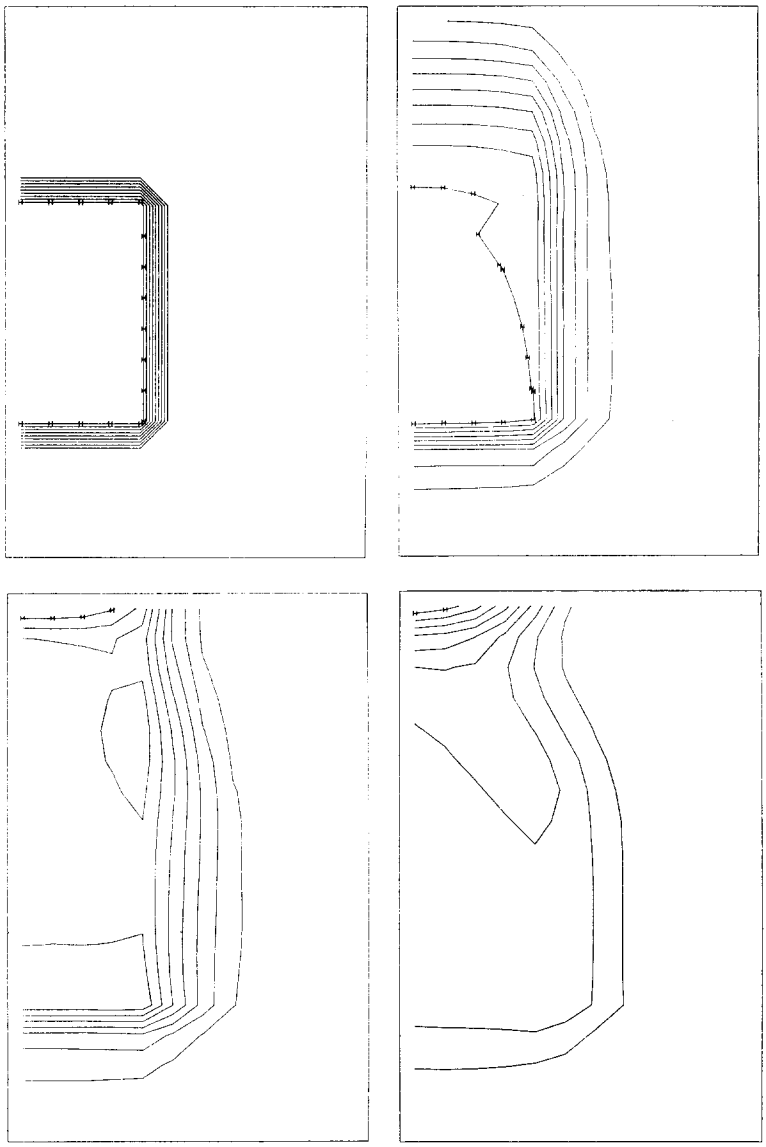

FIG. 4b. Plots of volume fraction θ for field 2.

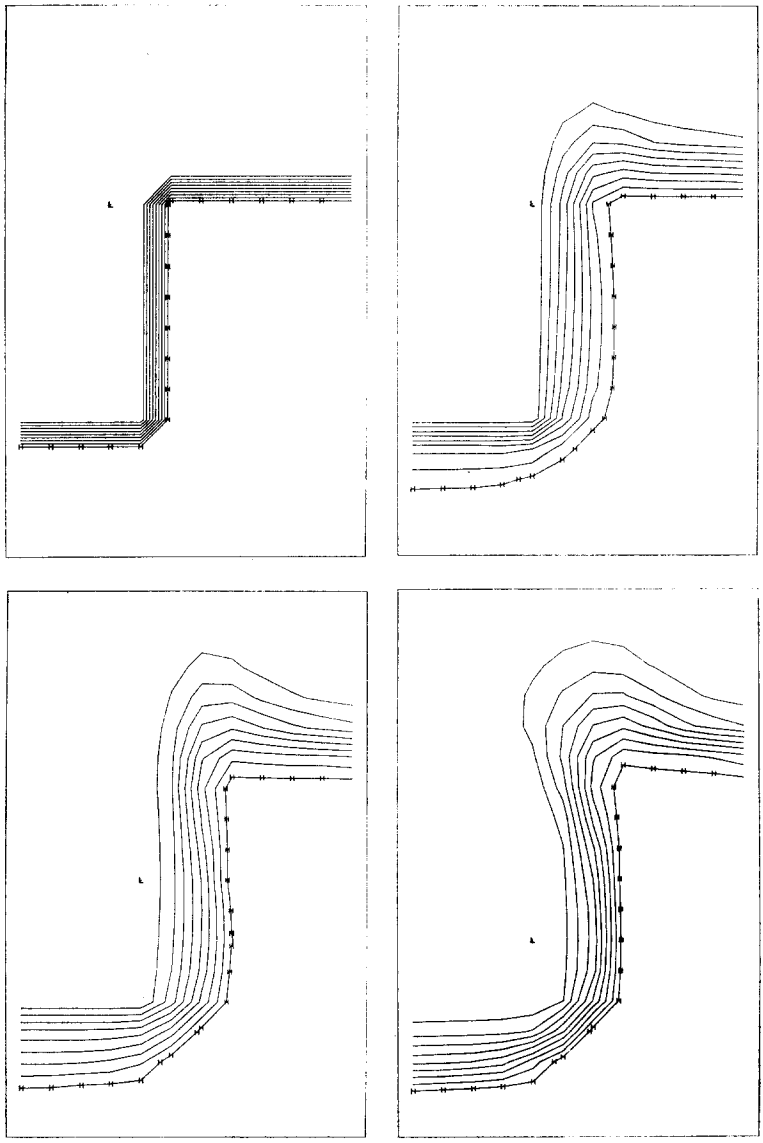

FIG. 4c. Plots of volume fraction θ for field 3.

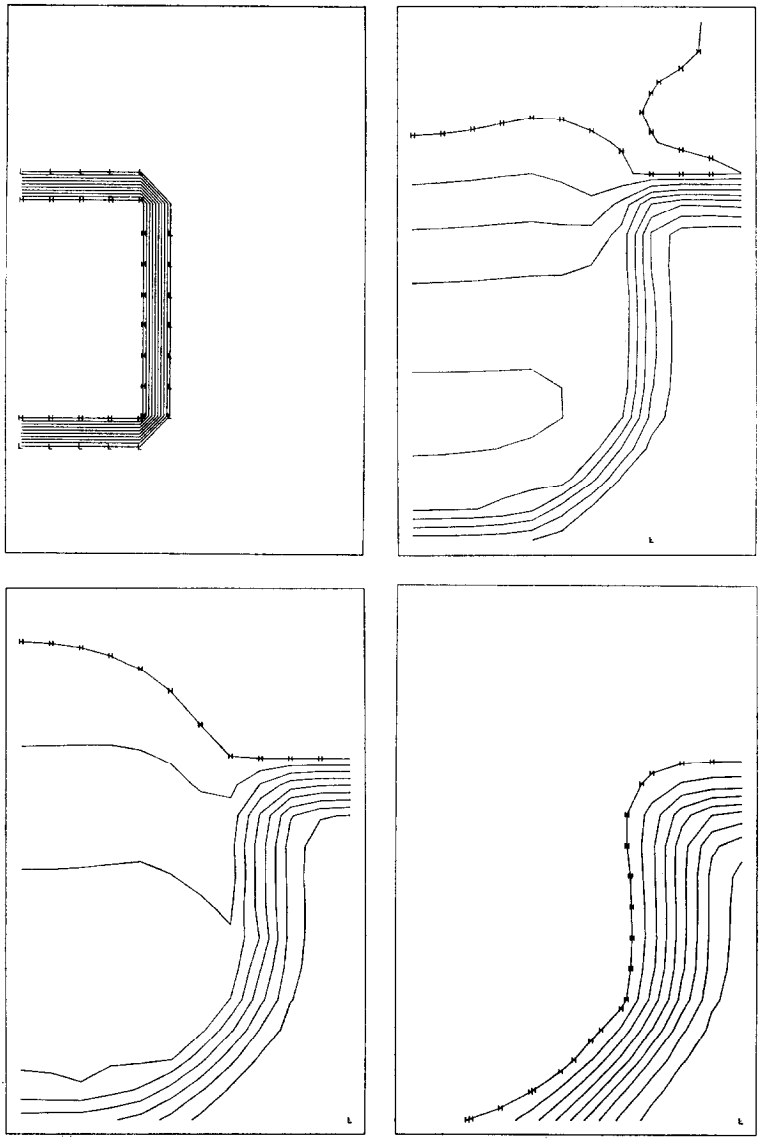

FIG. 5a. Plots of pressure for field 1.

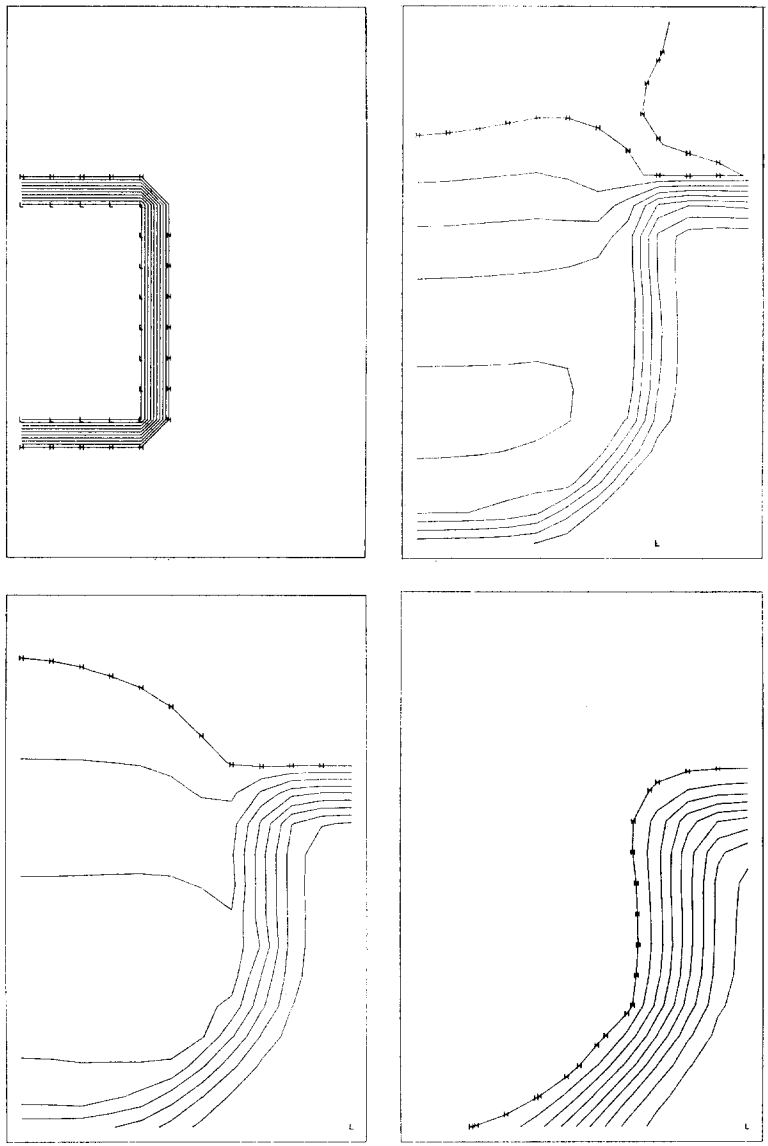

FIG. 5b. Plots of pressure for field 2.

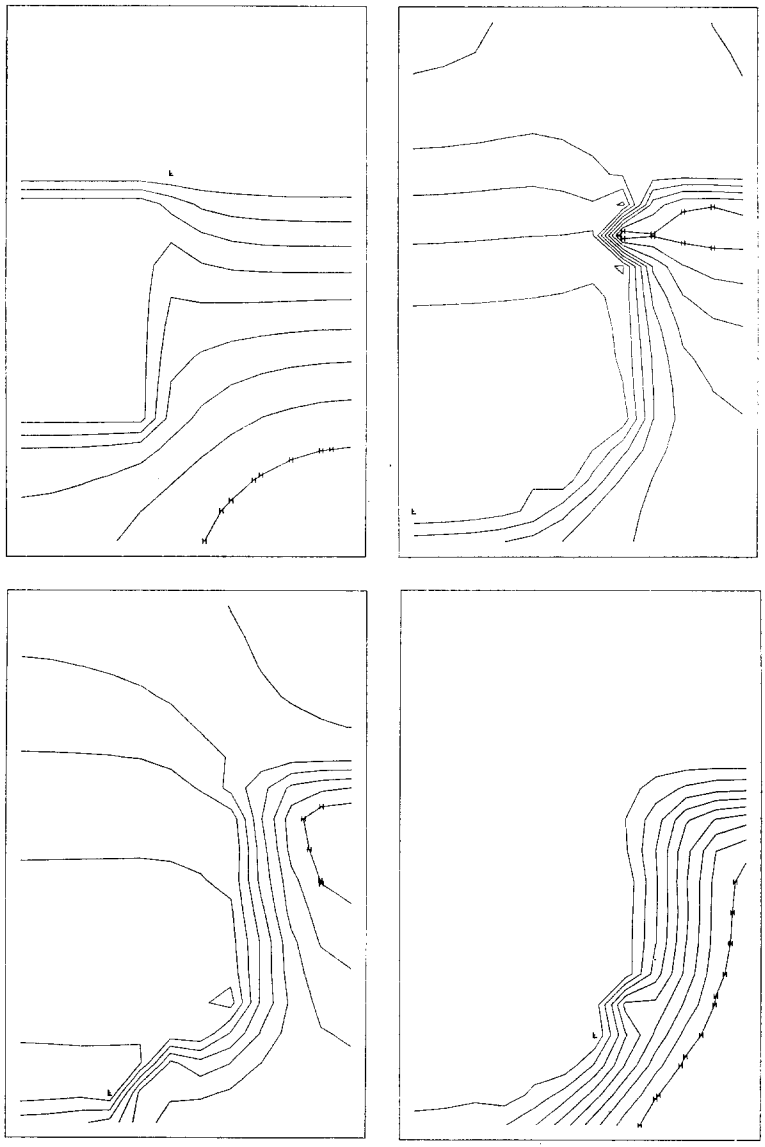

FIG. 5c. Plots of pressure for field 3.

Figure 2 shows marker particle configurations, with field 1 represented by the light dots, field 2 by the crosses, and field 3 by the open squares. The relative proportions of the number of marker particles of each type in a given region is governed by the initial θ for each field. This example employs comparatively few marker particles per unit area. Separate plots for each field are often appropriate for large numbers of particles, but the composite plots of particles from all fields, such as Fig. 2, are especially useful for showing relative motion and interpenetration of the various fields with time.

Figures 3a–3c show velocity vectors for fields 1–3, respectively, with each vector originating at a cell center, denoted by a cross. Each lies in the direction of the local flow, and has a length proportional to local velocity magnitude. Because each plot is scaled to the maximum velocity in the given field at that instant of problem time, only a qualitative comparison between separate plots can be made. At $t = 0.1$, the only significant velocities are those of the expanding vapor from the heated central core. The velocity magnitudes of fuel and iron, which are fairly tightly bound to one another through the drag function K_{23}, only build up to values comparable to those of the vapor by around $t = 50$, and thereafter decay to a fraction of the magnitude of the vapor velocity. An effect of the confining rigid walls of the system is the strong circulation patterns that are induced. Note that in a number of instances the direction of the vapor velocity vectors is directly opposite to that of the local fuel and iron.

Contours of the volume fraction θ are shown in the sequences of Figs. 4a–4c. In the contour plots, the H's denote the lines with highest algebraic value, and the L denotes the point in the mesh with lowest algebraic value. Contours of pressure are shown in Figs. 5a–5c. The effects of pressure equilibration are particularly apparent in the marked similarity between the plots for the two open fields, vapor (Fig. 5a), and fuel (Fig. 5b). Because the iron liner is initially close packed and has little opportunity to open significantly, the frames of Fig. 5c offer somewhat of a contrast to those of 5a and 5b.

REFERENCES

1. F. H. HARLOW AND A. A. AMSDEN, *J. Comp. Phys.* **17** (1975), 19; A. A. AMSDEN AND F. H. HARLOW, KACHINA: An Eulerian Computer Program for Multifield Fluid Flows, Los Alamos Scientific Laboratory report LA-5680 (1975).
2. J. R. TRAVIS, F. H. HARLOW AND A. A. AMSDEN, Numerical Calculation of Two-Phase Flows, Los Alamos Scientific Laboratory report LA-5942-MS (1975).
3. C. W. HIRT, *J. Comp. Phys.* **2** (1968), 339.
4. W. C. RIVARD, O. A. FARMER, T. D. BUTLER, AND P. J. O'ROURKE, A Method for Increased Accuracy in Eulerian Fluid Dynamics Calculations, Los Alamos Scientific Laboratory report LA-5426-MS (1973).